An Evaluation of Techniques for the Extraction of Mineral Absorption Features from High Spectral Resolution Remote Sensing Data

Michael Rast
European Space Agency, ESTEC, Noordwijk, The Netherlands
Simon J. Hook
Jet Propulsion Laboratory, California Institute of Technology, Pasadena, CA 91109
Christopher D. Elvidge
Desert Research Institute and Agricultural Experiment Station, University of Nevada System, Reno, NV 89506
Ronald E. Alley
Jet Propulsion Laboratory, California Institute of Technology, Pasadena, CA 91109

ABSTRACT: Airborne imaging spectrometer data are influenced by a number of external factors, which mask subtle absorption features that permit the identification of surface mineralogy. This paper examines a variety of techniques developed to remove those factors, which result from the solar irradiance drop off, atmospheric absorption, and topographic effects. The techniques investigated are the flat-field correction, log residuals, and corrections using the LOWTRAN 7 atmospheric transfer code. These techniques were applied to Airborne Visible/InfraRed Imaging Spectrometer (AVIRIS) data acquired over Cuprite, Nevada. The processed data were evaluated for their ability to display the diagnostic absorption features of three areas of known mineralogy. These areas are dominated by the minerals alunite, buddingtonite, and kaolinite. The spectral features observed in the manipulated data were compared against those observed in the original data. Results indicate that the data corrected using the LOWTRAN 7 atmospheric transfer code constrained with local weather station data were the most effective at displaying the diagnostic absorption features of the areas of known mineralogy and introduced the least number of artifacts into the data. Of the remaining techniques, log residuals was the next most effective, based on the previous criteria, and has the additional advantage of not requiring any external data.

INTRODUCTION AND OBJECTIVES

THE POTENTIAL OF HIGH SPECTRAL RESOLUTION remotely sensed data for mineralogical identification was first demonstrated by Hunt and his co-workers using laboratory spectrometers (e.g., Hunt, 1977).

The first airborne spectrometer data were collected in 1981 using a spectrometer developed by the GER Corporation (Chiu and Collins, 1978). This instrument acquired a continuous one-dimensional path (profile) along the flight line. The spectrum of each pixel in the profile, between 400 and 2400 nm, was recorded in 576 channels (Milton *et al.*, 1983; Marsh and McKeon, 1983). The first imaging device was the Airborne Imaging Spectrometer (AIS), developed by the Jet Propulsion Laboratory (JPL) (Goetz and Srivastava, 1985). This instrument acquired data in 128 spectral bands in the range from 1200 to 2400 nm and had a field of view (FOV) of 3.7 degrees (Vane and Goetz, 1985). Since then a variety of imaging instruments have been developed, both by commercial companies and research institutes.

In 1987 NASA began data acquisition with the Airborne Visible/Infrared Imaging Spectrometer (AVIRIS). AVIRIS is a grating spectrometer and covers the visible to shortwave infrared (SWIR) portion of the electromagnetic spectrum from 400 to 2450 nm in contiguous 10-nanometre-wide bands with an FOV of 30 degrees (Porter and Enmark, 1987). To improve the signal-to-noise (S/N) performance, the instrument has been under continuous technology modification and has shown a gradually improving performance over the last three years. These improvements have enhanced the detection and interpretation capabilities achievable with AVIRIS (Green, 1990).

In this paper, AVIRIS data covering the wavelength range between 2000 and 2400 nm were evaluated for their ability to display the diagnostic mineral absorption features of certain alteration minerals, using different data processing techniques. The wavelength region between 2000 and 2400 nm is particularly important for mineralogic identification because it contains the diagnostic features of hydroxyl and carbonate minerals (Hunt, 1977). These absorption features, however, are masked by a variety of external factors related to the instrument, atmosphere, and morphology of the terrain. This has resulted in the development of a variety of techniques to remove these artifacts. The techniques can be separated into two broad categories:

- Scene based techniques which use parameters derived from the data themselves. In this study the flat-field correction (described in Roberts *et al.* (1985)) and log residuals (described in Green and Craig (1985)) are the examples for scene based techniques.
- Correction techniques using external information like solar/atmospheric models. The LOWTRAN 7 model was used in this study with and without radiosonde data from the weather station at Desert Rock, located about 140 km southeast of the test site.

The AVIRIS data used here were acquired on 29 September 1989 at 11:25 AM (local time) over the Cuprite mining district, western Nevada. This area was selected for the study because of the presence of well exposed areas of alteration with pronounced variations in SWIR absorption features (Hook *et al.*; 1990, Kruse *et al.*, 1990).

The investigation is restricted to an area of approximately 5 by 5 km in which small sites of uniform mineral composition were chosen. Ground samples from these sites were acquired and analyzed with a laboratory spectrometer and by X-ray Diffraction (XRD) analysis. Particular emphasis was placed on the ability to identify the diagnostic absorption features of these alteration minerals. The investigation is favored by the fact that the alteration is well exposed, and vegetation is practically absent. The main objective of the study was to evaluate the effectiveness of several data processing techniques for the

PHOTOGRAMMETRIC ENGINEERING & REMOTE SENSING,
Vol. 57, No. 10, October 1991, pp. 1303–1309.

0099-1112/91/5710–1303$03.00/0

identification of mineralogical composition based on subtle differences in the spectral absorption features in the shortwave infrared.

LOCATION AND GEOLOGY OF THE STUDY AREA

The Cuprite area is located on the western edge of Esmeralda County, Nevada, along Mount Jackson Ridge about 25 km south of the town Goldfield. The study area is situated east of U.S. highway 95 and is composed exclusively of Tertiary volcanic rocks and Quaternary deposits.

The geologic map presented in Figure 1 is derived from an unpublished map by R.P. Ashley (1977). Descriptions of the geologic units have been drawn from Albers and Stewart (1972) and Ashley and Abrams (1980). The Tertiary volcanics were hydrothermally altered in the mid- to upper Miocene and the pattern of the hydrothermal alteration is well expressed as a central silicified zone, surrounded by an opalized zone with abundant kaolinite and alunite, with an outer ring of argillic alteration (Ashley and Abrams, 1980). Minor areas of alteration containing buddingtonite have been documented in the opalized zone (Goetz and Srivastava, 1985). Laboratory spectra combined with the results of an X-ray diffraction analysis of geological field samples were used for validating the results derived from the AVIRIS data sets.

PROCESSING TECHNIQUES

This investigation sought to examine various processing techniques which, when applied to a calibrated data set, permitted the identification of the diagnostic absorption features of the alteration minerals known to be at the site. The techniques were evaluated for their ability to correct for atmospheric influences while preserving the full spectral information and avoiding the introduction of artifacts by data handling.

The processing of the radiance data (as received by the sensor) to produce the calibrated data set supplied by the Jet Propulsion Laboratory is described in Reimer *et al.* (1987).

The calibrated data were processed using four techniques. These were

- Flat-field correction using a homogeneous, bright reflecting target area within the scene.
- Log-residual corrected data.
- LOWTRAN 7 correction, using the U.S. standard mid-latitude summer atmospheric values.
- LOWTRAN 7 correction, using Radiosonde data acquired at the same time as the data, to constrain the atmospheric transfer code.

Each of these processing techniques is designed to translate radiance into reflectance for comparison with laboratory- and field-derived spectra. The four techniques are described in detail below.

Flat-Field Correction

The purpose of the flat-field correction is to reduce the atmospheric influence in the data and eliminate the solar irradiance drop off, as well as any residual instrumental effects (not taken care of in the initial data calibration). This is achieved by dividing the whole data set by the mean value of an area within the scene, which is spectrally homogeneous, and spectrally and morphologically flat. Thus, the major absorption features caused by atmospheric influence and the "solar curve" effect, as well as system induced effects, are divided out.

The flat field chosen should have a high albedo to avoid the decreased S/N associated with low albedo flat fields. Ground truth knowledge of the surface material is necessary for the selection of the averaging area, which has to come close to an ideal, spectrally flat area. A flat-field correction was applied to the data set using the Stonewall Playa, a morphologically and spectrally flat surface in the eastern part of the test area.

The Log-Residual Correction

This technique is described in Green and Craig (1985) and removes the solar radiance drop off, atmospheric effects, and topographic effects in the data set. In this technique, the radiance measured by the sensor ($L_{i\lambda}$) is being related to the reflectance ($R_{i\lambda}$) in pixel i at wavelength λ by means of a multiplicative formula (Green and Craig, 1985); i.e.,

$$L_{i\lambda} = T_i R_{i\lambda} I_\lambda \quad (1)$$

The topographic factor (T_i) is constant for all wavelengths of a given pixel and accounts for brightness variations due to differences in angle and orientation of slope. The illumination factor (I_λ) describes the solar irradiance curve and is constant for all pixels at a given wavelength. By taking the logarithm of both sides and rearranging terms, the quantity ($\log R_{i\lambda}$), independent from topography and solar irradiance, can be derived. That is,

$$\log (R_{i\lambda}) = \log (L_{i\lambda}) - \log (T_i) - \log (I_\lambda) \quad (2)$$

where
- $\log (L_{i\lambda})$ = the log of the digital number value for pixel i at wavelength λ,
- $\log (T_i)$ = the average of the logs of pixel i for all wavelengths (one value per pixel), and
- $\log (I_\lambda)$ = the average of the logs of all pixels for a given wavelength (one value per channel).

Equation 2 summarizes the log residual calculation as described by Green and Craig (1985). In practice a fourth value has been added to this equation, the average of the logs of all samples at all wavelengths (one value per image). This fourth value normalizes the log-residual values from each flightline (Roberts *et al.*, 1985).

LOWTRAN 7 Corrected Data

During radiometric correction, the digital values (as recorded by the AVIRIS system) are converted into radiance values using the AVIRIS laboratory radiance calibration data. The LOWTRAN 7 model (Kneizys *et al.*, 1988) was applied to correct the AVIRIS flight data for atmospheric influence. This model was developed by the Air Force Geophysics Laboratory and predicts the atmospheric transmission and path radiance affecting the performance of optical surveillance tools. The model includes different geographical atmospheric profiles, as well as different aerosol models, humidity, and temperature profiles. The LOWTRAN 7 code provides many default values for its input parameters, assuming a U.S. standard atmosphere. In a previous investigation, carried out by Conel *et al.* (1987), the successful application of the LOWTRAN code to imaging spectroscopy data for atmospheric correction was demonstrated.

There were two possible ways to use LOWTRAN 7 in this investigation:

- Use only the date and time of the overflight plus the location of the site of investigation and run the model with the U.S. standard atmosphere inputs, contained in the model as default values for each season of the year and any latitude on the Earth.
- Constrain the atmospheric code with radiosonde data taken on the day and at approximately the time of the overflight. Ideally, this approach should be more accurate than assuming the standard atmosphere. The model, developed by Bosch and Alley (1990), was used to constrain the LOWTRAN 7 code and is described below.

It is assumed, that the observed radiance at the sensor (L_O) consists of the observed radiance due to path scattering (L_{PS}) and observed radiance due to ground reflected radiation (L_g). The solar radiance (L_R) multiplied by the ground reflectance (ρ) and the transmittance along downward and upward paths (t_1,

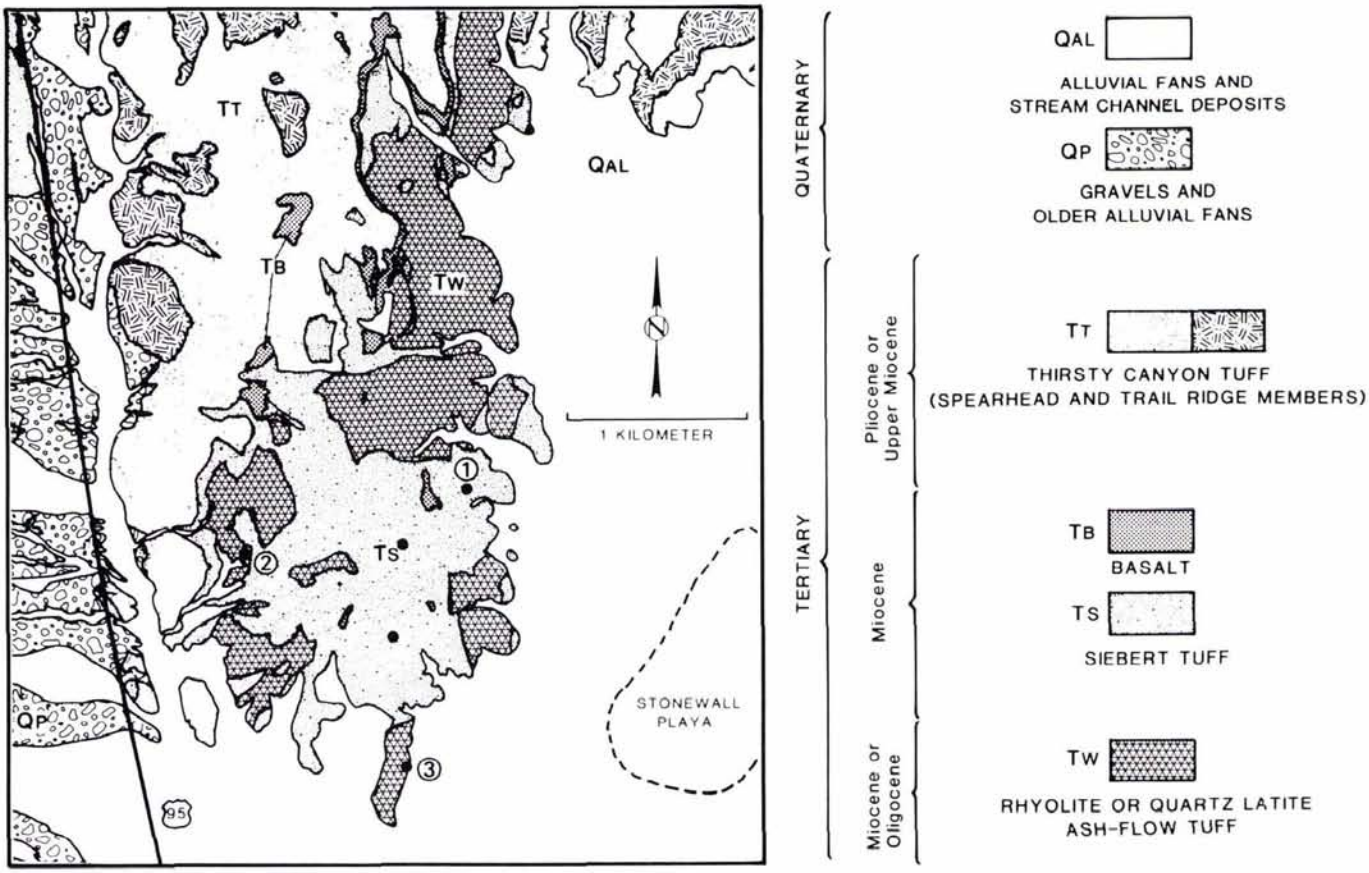

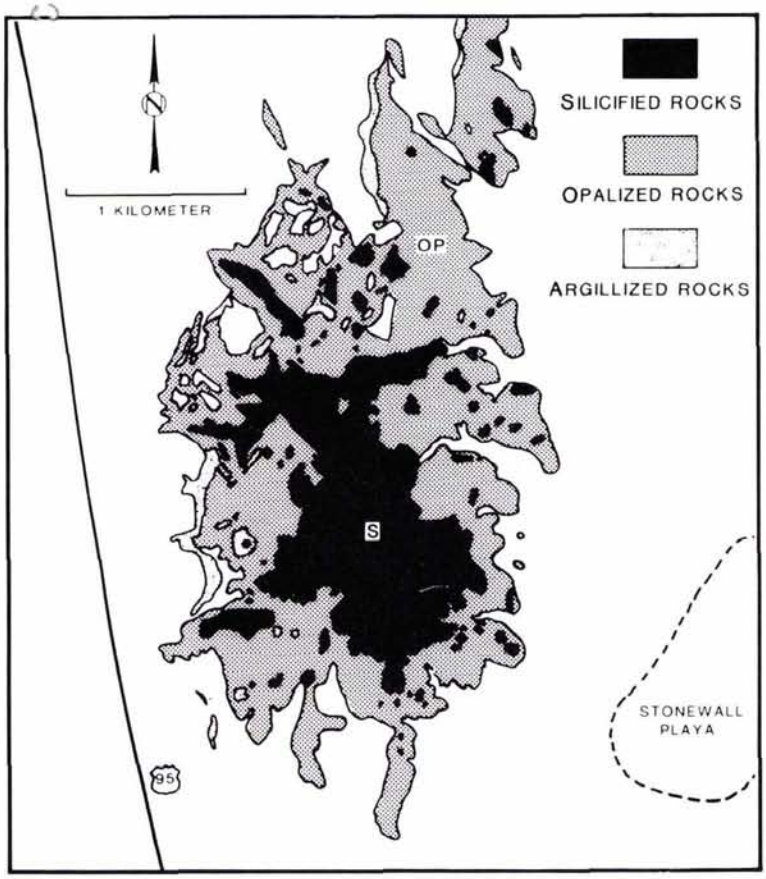

FIG. 1. Geology and alteration of the test area. The upper map shows the lithological setting; the lower map is a display of the alteration zones (after Ashley, 1977). Upper map: point 1 is the sampling location for alunite, 2 for buddingtonite, 3 for kaolinite.

t_2) corresponds to L_g. The observed radiance at the sensor can be formulated as

$$L_O = L_{PS} + L_g = L_{PS} + L_R t_1 \rho t_2 \quad (3)$$

Assuming a spectrally constant ground reflectance (0.1 in this case), LOWTRAN 7 can be used to model L_{PS} and L_g for the assumed reflectance. The ground reflectance can be expressed as

$$\rho = \frac{L_O - L_{PS}}{\left[\frac{L_g}{0.1}\right]} = \frac{0.1}{L_g}\,[L_O - L_{PS}] \quad (4)$$

Ground reflectance values can now be computed for each individual channel and applied for correcting the whole three-dimensional data set (Bosch and Alley, 1990).

In this study, the radiosonde data for Desert Rock (approximately 140 km southwest of Cuprite) were used to constrain the LOWTRAN 7 model. First, the values for path radiance and surface reflection are calculated for each wavelength in the data set. For this purpose, the AVIRIS response function and channel position have to be calculated into LOWTRAN 7 in order to make the spectral resolution and the response compatible between the model and the spectrometer.

The values created as correction factors for each channel are reproduced by the number of lines and samples in order to generate the correction values per band in an image format. Then the two data sets (image data and LOWTRAN 7 data) are multiplied pixel by pixel for each wavelength channel. Thus, the raw data are corrected for atmospheric influence throughout the whole data set.

LABORATORY MEASUREMENTS

Field samples from the investigated area were collected in October 1989. The composition of these samples was determined by laboratory spectrometry and XRD. The laboratory hemispherical reflectance spectra were acquired with a Beckman UV 5240 spectrometer. The XRD analyses were done using a SCINTAG XDS-2000 automated diffractometer.

In order to evaluate the techniques described above, three areas dominated by the alteration minerals—alunite, buddingtonite, and kaolinite—were selected as test cases. For each of the three areas, the spectrum of one pixel which, according to field observation and sample analysis, was dominated by one of the three alteration minerals was extracted and the spectrum obtained after processing with each technique was compared.

In addition, for the kaolinite area, a 3- by 3-pixel average was obtained, in order to demonstrate that scene inherent noise and topographic surface inhomogeneities can be reduced considerably by averaging over a larger area. The Cuprite test site is, due to its large and uniform alteration zones, very well suited for spatial averaging. The kaolinite occurrence at the location "Kaolinite Hill" (see Figure 1 upper map point 3) extends over a large area.

A brief discussion of the minerals selected for the investigation is given below:

ALUNITE

Alunite [$KAL_3(SO_4)_2(OH)_6$] is widespread in rocks that have been altered by sulfuric acid bearing solutions derived from volcanic gases or the weathering of sulfide minerals (Hunt *et al.*, 1971). The two most prominent absorption features in the SWIR occur at 2180 nm appearing as a doublet with the second, weaker absorption feature at 2210 nm. A second broad absorption appears at 2320 nm. These features are due to OH frequency stretching (Hunt *et al.*, 1971) (Figure 2).

BUDDINGTONITE

Buddingtonite [$NH_4AlSi_3O_8 \cdot nH_2O$] is an ammonium aluminum silicate hydrate. Described as an ammonium feldspar analogous to orthoclase, it was the first naturally occurring ammonium aluminosilicate to be described (Erd *et al.*, 1964). Buddingtonite can occur as a replacement mineral in hydrothermally altered andesite, where ammonium, NH_4^+ substitutes for K^+ or other alkali cations bound within the crystal structure (Krohn and Altaner, 1987). Buddingtonite shows a broad and strong vibrational absorption feature due to NH_4 around 2120 nm (Krohn and Altaner, 1987).

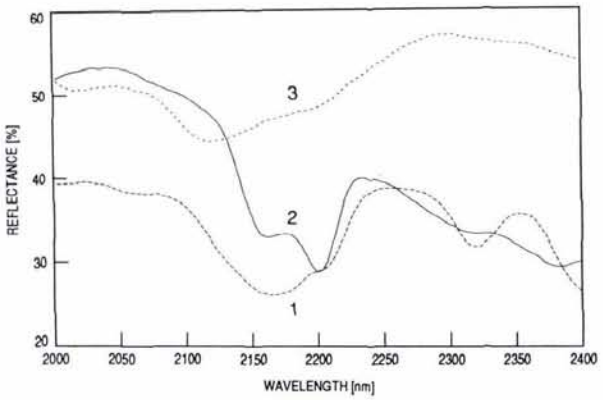

FIG. 2. Beckman laboratory spectrometer reflectance spectra of alunite (1), kaolinite (2), and buddingtonite (3) taken from the field samples.

KAOLINITE

Kaolinite [$Al_2Si_2O_5(OH)_4$] is formed as a weathering product by hydrothermal alteration or as an authigenic sedimentary mineral (Murray, 1988). Its spectrum is dominated by strong hydroxyl absorption bands which are in the shortwave infrared between 2150 nm and 2200 nm (Hunt and Salisbury, 1970). The OH absorption appears in the form of a doublet, the weaker absorption occurring at about 2160 nm, the stronger absorption feature at 2200 nm. Further out in the SWIR another absorption feature can be detected at 2320 nm (Figure 2).

RESULTS

In the Figures 3(a)1–5, 3(b)1–5, and 4(a)1–5 always one-pixel spectra of the SWIR are shown after processing using the techniques described above. The graphs of the figures correspond to

(1) the original calibrated radiance data,
(2) the flat-field corrected data,
(3) the log-residual corrected data,
(4) the LOWTRAN 7 corrected data assuming the standard atmosphere default values, and
(5) the LOWTRAN 7 corrected data constrained with radiosonde input.

As mentioned above, the pixels selected for the display of the spectra are dominated by one mineral. These are alunite in Figure 3(a); buddingtonite in Figure 3(b); and kaolinite in Figures 4(a) and 4(b).

Figure 4(b) shows the average kaolinite spectrum from an area of 3 by 3 pixels. In Figures 3(a) and 3(b) and in Figure 4(a) the solid line represents the actual spectrum in its intensity versus the wavelength. The dashed line is a three-channel moving average filtered spectrum, offset by about 10 to 15 percent from the original spectrum (solid line) for reasons of clarity. These averaged spectra were produced for each single pixel spectrum with the purpose of smoothing the spectral curve and reducing the noise contained in the observed pixel, due to the fact that the AVIRIS has a relatively low S/N in the SWIR (Hook *et al.*, 1990). Even though the main absorption features are well

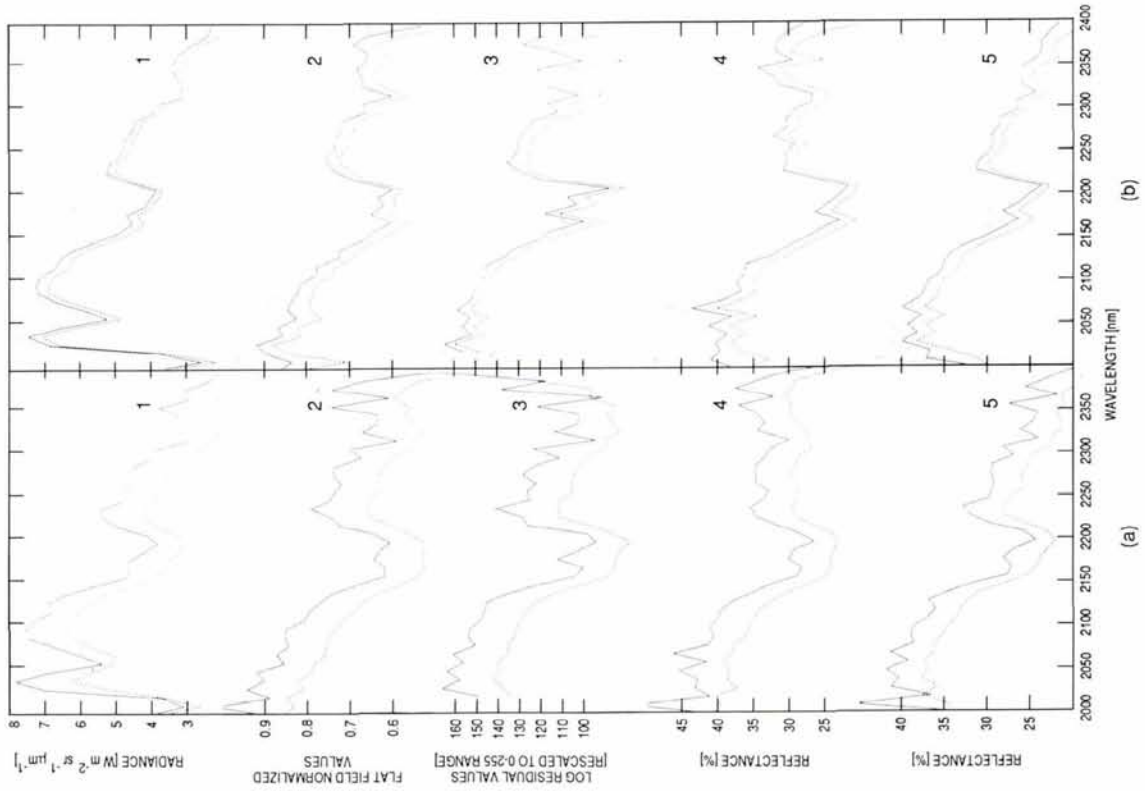

FIG. 4. Mineral spectra of kaolinite.

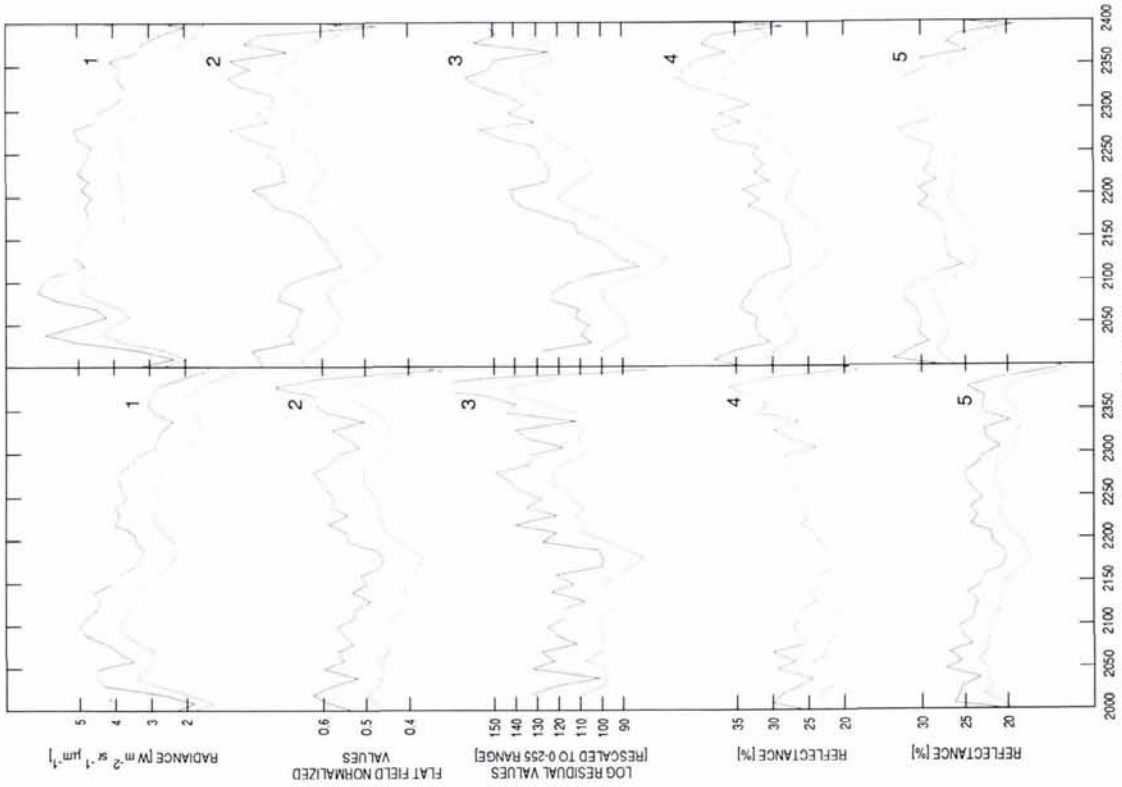

FIG. 3. Mineral spectra of alunite and buddingtonite.

preserved and noise has been reduced, some subtle but important features, like the doublet (weaker twin absorption feature, contained in a major absorption) in the kaolinite spectrum (at 2180 nm) and, in particular, in the alunite spectrum (at 2200 nm), are suppressed as is apparent in Figures 3(a)1 and 3(a)5 and Figure 4(a)1. Consequently, the main emphasis in the evaluation of the data has been directed towards the spectrally unfiltered data.

The different spectra are discussed below.

Alunite, Figure 3(a)

In order to ensure a correct interpretation, all data within one processing technique were displayed at the same graphical scale. Therefore, alunite shows a less drastic expression in its absorption features (as compared to kaolinite) and is dominated by weak minima that would be more clear, if an expanded scale were applied. Nevertheless, the calibrated data (Figure 3(a)1) as well as the LOWTRAN 7 radiosonde-corrected data (Figure 3(a)5) show the alunite doublet between 2200 nm to 2210 nm. In the LOWTRAN 7 standard correction (Figure 3(a)4) as well as in the flat field corrected data (Figure 3(a)2) a reasonable distinction of the main absorption feature at 2180 nm from the noise is difficult. The log residual data (Figure 3(a)3) do exhibit the main absorption feature even though the process does introduce noise. The second significant absorption feature of alunite at 2320 nm is, with the exception of the calibrated data (Figure 3(a)1), not very well distinguishable from the noise with all the processing techniques. However, the absorption can be seen in the spectrally filtered dashed spectra in all of the data sets.

Buddingtonite, Figure 3(b)

The broad absorption of buddingtonite at 2120 nm is apparent in all of the manipulated products, with the exception of the calibrated data. This is due to atmospheric influence that is not compensated for. Atmospheric influence is also responsible for the difference between the flat field (Figure 3(b)2) and both the LOWTRAN 7 corrected spectra (Figures 3(b)4 and 3(b)5). Because the compensation cannot be achieved accurately by the atmospheric models at this particular wavelength, the flat-field correction, in this case, seems to eliminate the H_2O absorption around 2100 nm best. Also, the LOWTRAN 7 radiosonde corrected data in Figure 3(b)5 show a better result than the standard atmosphere constrained data (Figure 3(b)4). As in the case of alunite, the log residuals (Figure 3(b)3) emphasize the main absorption features at 2120 and at 2300 nm, the latter also being detectable in the other buddingtonite data sets. An additional feature is introduced at around 2230 nm. This absorption may result from the scene average that is dominated by hydroxyl absorption features around 2200 nm. These would elevate the spectra of pixels that do not contain the dominant material around 2200 nm, introducing an artificial drop-off at longer wavelengths (Hook *et al.*, 1990).

Kaolinite, Figure 4(a)

Kaolinite shows the most distinct spectrum of all the minerals and is well suited for comparing the different processing techniques. The kaolinite doublet (at 2180 nm) is detectable in all the data products (Figure 4(a)1 to 4(a)5), with the log residuals (Figure 4(a)3) again showing the strongest emphasis of the feature in spite of the introduced noise. Apart from that, the radiosonde constrained LOWTRAN 7 data (Figure 4(a)5) show, having corrected for the atmospheric influence, the best result besides the calibrated data. The LOWTRAN 7 standard data and the flat-field corrected set do not portray the decrease in reflection from kaolinite at wavelengths beyond 2250 nm as can be seen in the laboratory spectrum, measured from the field sample by the Beckman spectrometer (solid curve in Figure 5). Minor noise is also being introduced in this case by the radiosonde constrained LOWTRAN 7 data. Nevertheless, the major atmospheric absorption features at 2060 and 2330 nm are well corrected for.

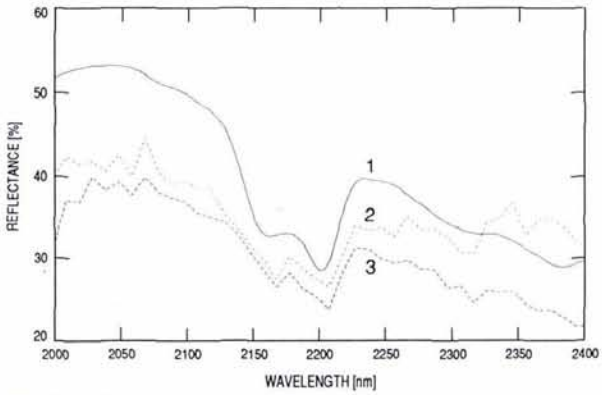

Fig. 5. Reflectance spectra from the Lab spectrometer (solid line, 1), the LOWTRAN 7 transfer code using standard atmospheric conditions (2), and the LOWTRAN 7 code using radiosonde data as input (3).

Kaolinite—Averaged Area, Figure 4(b)

Figure 4(b) demonstrates how noise, together with inhomogeneities in the spectrum, can be reduced as soon as a bigger area of uniform adjacent pixels are averaged. Here the average of a 3- by 3-pixel area has been calculated from the processed data. In all cases in Figure 4(b), the dotted lines above and below the solid spectral curve (mean value of the nine pixels) represent the spectral mean value plus and minus one standard deviation in order to show the error range, when applying such a spatial average. All of the data sets clearly demonstrate the reduction of noise and inhomogeneities, while again only the calibrated (Figure 4(b)1) and the radiosonde constrained LOWTRAN 7 data (Figure 4(b)5) display the decrease in reflection beyond 2250 nm. For both the flat-field corrected data (Figure 4(b)2) as well as the log residuals (Figure 4(b)3), an additional feature is introduced into the kaolinite doublet. In Figure 5 the previously mentioned field sample spectrum of kaolinite is shown together with the two LOWTRAN 7 data products in one diagram. Because the LOWTRAN 7 data are reduced to reflectance values, they can be compared to the laboratory reflectance data. The solid line 1 represents the lab spectrum, spectral curve 2 represents the standard atmosphere constrained LOWTRAN 7 data set, and curve 3 the radiosonde constrained one. For both cases, again in order to reduce noise and inhomogeneity, the 3- by 3-pixel averaged sample has been chosen as example. A clear correlation between the radiosonde constrained data and the lab spectrum can be detected. The difference in signal levels is due to the signal losses in the system and the influence of some silica, present in the observed nine pixels, that suppresses to a certain extent the distinctiveness of the kaolinite absorption features. Meanwhile, the lab measured field sample taken from that area and measured in the laboratory shows in the XRD analysis an abundance of kaolinite. The LOWTRAN 7 data set, that is constrained by the standard atmosphere default values, shows only a clear overcompensation of the atmospheric influence, obvious from the fact that it crosses the lab spectrum. For detailed mineral analysis in the SWIR, a very accurate correction of the atmospheric influence is necessary. For this, the standard default LOWTRAN 7 values appear to be unsatisfactory for the analysis of remotely sensed spectrometry data.

SUMMARY AND CONCLUSIONS

At this point it has to be emphasized that, even though many of the features are detectable in the calibrated original data in the SWIR, the atmospheric influence has to be corrected in order to guarantee a relatively accurate match of the lab spectrum with the image derived spectrum.

Apart from the calibrated original data, the radiosonde constrained LOWTRAN 7 processed data show the best results for determining the trend of a spectrum including secondary absorption features. Thus, they are to be given preference over the standard atmospheric values in the LOWTRAN 7 method. The disadvantage here is that radiosonde data of the area of observation have to be provided.

For identification, using scene based techniques, without external information, the log residuals clearly show the best results. As demonstrated several times throughout the investigation, the log residuals impressively emphasize, despite the noise introduced by the technique, the major absorption features of the present minerals.

The flat-field correction shows the least satisfactory results of the scene based techniques used, not only because of the noise introduced with the technique, but also because of the necessity of having a spectrally and morphologically flat and preferably bright reflecting target contained in the scene to carry out the correction. In the present study, the correction area used as a flat field (the Stonewall Playa) shows some minor carbonate absorption features which are, through the correction process, divided into the whole scene and thus falsify the results to a certain extent.

Summarizing, it can be said that the log residuals technique gives the best results of the scene based techniques, while the LOWTRAN 7 radiosonde constrained correction offers the best results of the techniques examined. In the present case, where a homogeneous area was being investigated, a spatial average of 3 by 3 pixels enhanced the results and the resemblance to the laboratory data by reducing noise and inhomogeneities on the pixel scale. An averaging in the spectral domain, however, has led to the suppression not only of noise but also of smaller absorption features, vital for mineral identification.

ACKNOWLEDGMENTS

Discussions with Mike Abrams on the approach used in these analyses are gratefully acknowledged. The authors would also like to thank Cindy Grove and H. N. Paley of the Jet Propulsion Laboratory, who gave of their time and ideas in many discussions of the work, and Dennis Joseph of the National Center of Atmospheric Research (NCAR) for providing the Radiosonde data from Desert Rock.

The research described in this paper was carried out while the first author held the scientific "Douglas Marsh Fellowship" granted by the European Space Agency at the Jet Propulsion Laboratory, California Institute of Technology, under contract to the National Aeronautics and Space Administration.

REFERENCES

Albers, J. P., and J. H. Stewart, 1972. Geology and Mineral Deposits of Esmeralda County, *Nevada*, Nevada Bureau of Mines and Geology, Bulletin 78.

Ashley, R. P., and M. J. Abrams, 1980. *Alteration mapping using multispectral images—Cuprite mining district, Esmeralda County, Nevada*, U.S. Geological Survey, Open File Report 80-367.

Ashley, R. P., 1977. *Geologic map and alteration map, Cuprite Mining District, Nevada* (unpublished).

Bosch v.d., J. M., and R. E. Alley, 1990. "Application of LOWTRAN 7 as an atmospheric correction for Airborne Visible/Infrared Imaging Spectrometer (AVIRIS) data," presented at the second AVIRIS workshop at the JPL, June 1990.

Chiu, H. Y., and W. E. Collins, 1978. A spectroradiometer for airborne remote sensing, *Photogrammetric Engineering & Remote Sensing*, Vol. 44, pp. 507-517.

Conel, J. E., R. O. Green, C. J. Bruegge, and R. E. Alley, 1987. Airborne Imaging Spectrometer-2: Radiometric spectral characteristics and comparison of ways to compensate for the atmosphere, *SPIE Proc., Imaging Spectroscopy II*, Vol. 834, (G. Vane, editor), pp. 140-157.

Erd, R. C., D. E. White, J. J. Fahey, and D. E. Lee, 1964. Buddingtonite, an ammonium feldspar with zeolithic water, *Am. Mineral.*, Vol. 49, pp. 831-850.

Goetz, A. F. H., and V. Srivastava, 1985. Mineralogical mapping in the Cuprite Mining District, Nevada, *Proceedings of the Airborne Imaging Spectrometer Data Analysis Workshop* (G. Vane and A. F. H. Goetz, editors). JPL Pub. 85-41, Jet Propulsion Lab., Pasadena, Calif., pp. 22-31.

Green, A. A., and M. D. Craig, 1985. Analysis of aircraft spectrometer data with logarithmic residuals, *Proceedings of the Airborne Imaging Spectrometer Workshop*, (G. Vane and A. F. H. Goetz, editors). JPL Publication 85-41, JPL, Pasadena, Calif. pp. 111-119.

Green, R. O., J. E. Conel, J. S. Margolis, V. Carrere, C. J. Bruegge, M. Rast, and G. Hoover, 1990. In-flight validation and calibration of the spectral and radiometric characteristics of the Airborne Visible/Infrared Imaging Spectrometer, *SPIE Proc., Imaging Spectroscopy of the Terrestrial Environment* (G. Vane, editor), Vol. 1298, pp. 18-36.

Hook, S., C. D. Elvidge, M. Rast, and H. Watanabe, 1990. Evaluation of the mineral absorption features in short wave infrared (SWIR) data from the AVIRIS and GEOSCAN instruments at Cuprite, Nevada (submitted to *Journal of Geophysical Research*).

Hunt, G. R., 1977. "Spectral signatures of particulate minerals in the visible and near infrared", *Geophysics*, Vol. 42, No. 3, pp. 501-513.

Hunt, G. R., and J. W. Salisbury, 1970. Visible and near infrared spectra of minerals and rocks: I silicate minerals, *Modern Geology*, Vol. 1, pp. 283-300.

Hunt, G. R., J. W. Salisbury, and C. J. Lenhoff, 1971. Visible and near infrared spectra of minerals and rocks: IV. sulfides and sulfates, *Modern Geology*, Vol. 3, pp. 1-14.

Kneizys, F. X., G. P. Anderson, E. P. Shettle, W. O. Gallery, L. W. Abreu, J. E. A. Selby, J. H. Chetwynd, and S. A. Clough, 1988. *Users Guide to LOWTRAN 7*, Air Force Geophysics Laboratory, Hanscom AFB, Massachusetts, AFGL-TR-88-0177.

Krohn, M. D., and S. P. Altaner, 1987. Near infrared detection of ammonium minerals, *Geophysics*, Vol. 52, No. 7, pp. 924-930.

Kruse, F. A., K. S. Kierein-Young, and J. W. Boardman, 1990. Mineral mapping at Cuprite, Nevada with a 63-channel imaging spectrometer, *Photogrammetric Engineering & Remote Sensing*, Vol. 56, pp. 83-92.

Marsh, S. E., and J. B. McKeon, 1983. Integrated analysis of high resolution field and airborne spectroradiometer data for alteration mapping, *Economic Geology*, Vol. 78, No. 4, pp. 618-632.

Milton, N. M., W. C. Collins, S. H. Chang, and R. G. Schmidt, 1983. Remote Detection of metal anomalies on pilot mountain, Randolph County, North Carolina, *Economic Geology*, Vol. 78, No. 4, pp. 605-617.

Murray, H. H., 1988. Kaolin minerals: Their genesis and occurrences, Chapter 4 in *Reviews in Mineralogy*, Vol. 19, Hydrous Phyllosilicates (exclusive of micas), (S. W. Bailey, editor), Min. Soc. of America, pp. 67-89.

Porter, W. M., and H. T. Enmark, 1987. A system overview of the Airborne Visible/Infrared Imaging Spectrometer (AVIRIS), *Airborne Visible/Infrared Imaging Spectrometer (AVIRIS)*, (G. Vane, editor), JPL Pub. 87-38, pp. 3-12.

Reimer, J. H., J. R. Heyada, S. C. Carpenter, W. T. S. Deich, and M. Lee, 1987. Airborne Visible/Infrared Imaging Spectrometer (AVIRIS) ground data processing system, *SPIE Proceedings, Imaging Spectroscopy II*, (G. Vane, editor). Vol. 834, pp. 79-90.

Roberts, D. A., Y. Yamaguchi, and R. J. P. Lyon, 1985. Comparison of various techniques for calibration of AIS data, *Proc. of the 2nd Airborne Imaging Spectrometer Data Analysis Workshop* (G. Vane and A. F. H. Goetz, editors), JPL Pub. 86-35, pp. 21-30.

Vane, G., and A. F. H. Goetz, 1985. Introduction to the proceedings of the Airborne Imaging Spectrometer (AIS) Data Analysis workshop, *Proceedings of the Airborne Imaging Spectrometer (AIS) Data Analysis Workshop* (G. Vane and A. F. H. Goetz, editors), JPL Pub. 85-41.

(Received 20 August 1990; accepted 9 November 1990; revised 19 December 1990)